International Journal of Thermal Sciences 48 (2009) 2203–2214

Contents lists available at ScienceDirect

International Journal of Thermal Sciences

journal homepage: www.elsevier.com/locate/ijts

Modelling of roughness effects on heat transfer in thermally fully-developed laminar flows through microchannels

G. Gamrat [1], M. Favre-Marinet*, S. Le Person

Laboratoire des Ecoulements Géophysiques et Industriels, CNRS-UJF-INPG, 1025 rue de la Piscine, BP 53 X, 38041 Grenoble Cedex, France

ARTICLE INFO

Article history:
Received 20 November 2008
Received in revised form
30 March 2009
Accepted 13 April 2009
Available online 19 May 2009

Keywords:
Laminar flow
Heat transfer
Roughness
Microchannel
Numerical modelling

ABSTRACT

In this paper, roughness was modelled as a pattern of parallelepipedic elements of height k periodically distributed on the plane walls of a microchannel of height H and of infinite span. Two different approaches were used to predict the influence of roughness on heat transfer in laminar flows through this microchannel. Three-dimensional numerical simulations were conducted in a computational domain based on the wavelength λ. A one-dimensional model (RLM model) was also developed on the basis of a discrete-element approach and the volume averaging technique. The numerical simulations and the rough-layer model agree to show that the Poiseuille number Po and the Nusselt number Nu increase with the relative roughness. The RLM model shows that the roughness effect may be interpreted by using effective roughness heights k_{eff} and $k_{\mathrm{eff}\theta}$ for predicting Po and Nu respectively. k_{eff} and $k_{\mathrm{eff}\theta}$ depend on two dimensionless local parameters: the porosity of the rough-layer and the roughness height normalized with the distance between the rough elements. The present results show that roughness increases the friction factor more than the heat transfer coefficient (performance evaluation criteria < 1), for a relative roughness height expected in the fabrication of microchannels ($k/(H/2) < 0.46$) or $k/D_{\mathrm{h}} < 0.11$).

1. Introduction

The present study is devoted to the problem of heat transfer in laminar flow through rough-wall microchannels. Due to their impact in technology applications, flows in microchannels have been extensively studied and several aspects specific of microflows including roughness effects have been investigated in the recent years. A review may be found, for example, in Morini [1]. Several experimental studies have shown that the surface roughness increases the resistance to the flow, which is characterized by the Poiseuille number ($Po = fRe$, where f is the Fanning friction factor and Re is defined with the bulk velocity and the hydraulic diameter D_{h}). For example, Mala and Li [2] observed a moderate increase in Po ($\approx$10–20%) in fused silica or stainless steel microtubes ($D_{\mathrm{h}} = 50$–$254\ \mu\mathrm{m}$), when the relative roughness (k/D_{h}) was in the range 0.007–0.035. Pfund et al. [3] measured the pressure drop in deionized water flow through high aspect ratio rectangular microchannels made in a sandwich structure. When one of the walls of the 257 μm deep test section was a rough polyamide plate ($k/D_{\mathrm{h}} = 0.0075$), Po exhibited a significant increase ($\sim$25%) above the value Po_{smooth} obtained with smooth walls. An increase of up to 37% was found for Po by Li et al. [4] in rough stainless steel microtubes ($D_{\mathrm{h}} = 128.8$–$179.8\ \mu\mathrm{m}$, $k/D_{\mathrm{h}} = 0.03$–0.043). A more complete review on the hydrodynamics of laminar flows in rough microchannels may be found in Gamrat et al. [5].

Heat transfer experiments in microchannels are much more difficult than experiments on the flow hydrodynamics. As a consequence, the published results on heat transfer exhibit a large dispersion as pointed out by Sobhan and Garimella [6], who listed many possible sources of error in interpreting experimental data (entrance effects, axial conduction, roughness effects, non-uniformity of channel dimensions, thermal and flow boundary conditions, uncertainties and errors in instrumentation). In an attempt to identify specific roughness effects, several studies have considered heat transfer in rough-wall microchannels ([4,7–14], Table 1). All the referenced works used roughness resulting from the fabrication process of the microchannels, except Kandlikar et al. [9] who used tubes specially etched by acid to increase the surface roughness. Several microchannels with either smooth or rough-wall conditions were investigated in some studies [7,9,14]. In this case, Table 1 presents the measured Nusselt number referred to the value Nu_{smooth} obtained with a smooth microchannel in the same work.

* Corresponding author. Tel.: +33 4 76 82 50 49; fax: +33 4 76 82 52 71.
E-mail address: michel.favre-marinet@hmg.inpg.fr (M. Favre-Marinet).
[1] Present address: Institute of Aviation, Al. Krakowska 110/114, 02-256 Warsaw, Poland.

1290-0729/$ – see front matter © 2009 Elsevier Masson SAS. All rights reserved.
doi:10.1016/j.ijthermalsci.2009.04.006

Nomenclature

C_d	drag coefficient, –
C_p	specific heat at constant pressure, J kg^{-1} K^{-1}
C_r	resistance coefficient, –
D_h	hydraulic diameter, μm
d	side length of a rough element, μm
F	($=1/L^{*2}$), roughness structure fractionation ratio, –
f	Fanning friction factor, –
H	channel spacing, μm
H_s	thickness of the substrate, μm
h	convection heat transfer coefficient, W m^{-2} K^{-1}
k	roughness height, μm
k_{eff}	effective roughness height for friction (Eq. (57)), μm
$k_{eff\theta}$	effective roughness height for heat transfer (Eq. (61)), μm
$k_{f,s}$	fluid/solid thermal conductivity, W m^{-1} K^{-1}
L	distance between two successive rough elements (Fig. 2), μm
$\dot{m}$	mass flow rate per unit transverse length, kg m^{-1} s^{-1}
Nu	Nusselt number, –
Nu_{conv}	Nusselt number for fully-developed laminar flow between smooth parallel plates heated at uniform heat-flux, –
$Nu_d(y)$	local Nusselt number at the lateral side of a rough element, –
p	pressure, N m^{-2}
Pe	Peclet number, –
PEC	performance evaluation criteria, –
Po	Poiseuille number, –
Pr	Prandtl number, –
Re	Reynolds number, –
$Re_d(y)$	local Reynolds number (Eq. (18)), –
T	temperature, K
T_m	fluid bulk temperature, K
$\vec{u}$	velocity vector, m s^{-1}
u_b	bulk velocity, m s^{-1}
X	abscissa along the channel, m
x	local abscissa, m
y	coordinate in the direction perpendicular to the channel walls, m
z	coordinate in the spanwise direction, m

Greek symbols

ε	porosity, –
θ	dimensionless temperature (Eq. (14)), –
$\Lambda = k_s/k_f$	ratio of solid to fluid conductivity, –
ρ	density, m^3 s^{-1}
μ	dynamic viscosity, kg m^{-1} s^{-1}
φ_0	uniform heat-flux at the external side of the substrate, W m^{-2}
$\varphi(y)$	locally averaged heat-flux at the lateral side of a rough element, W m^{-2}
φ_{top}	heat-flux at the top surface of a rough element, W m^{-2}

Subscripts

app	apparent
f	fluid
s	solid

Superscripts

$(\cdot)^*$	non-dimensionalized by $H/2$
$\langle q \rangle$	superficial average of q
$\langle q \rangle^f$	intrinsic average of q in the fluid
$\langle q \rangle^s$	intrinsic average of q in the solid
$\tilde{q}$	periodic component of q

In other studies, the Nusselt number was not measured with smooth-wall conditions. The authors then compared the measured Nusselt number to the value Nu_{conv} expected in laminar flow through a smooth channel of identical geometry, as given by classical correlations [8,10,12,13] or their own numerical simulations [4,11]. It must be remarked that the measured Nusselt number may be affected by other effects than roughness and in the latter case, this is not accounted for by the ratio Nu/Nu_{conv}. Table 1 and Fig. 1 show that there is no agreement between the published experimental results and that even the tendencies are in disagreement. It

Table 1
Summary of experimental works on heat transfer in rough microchannels in the literature.

Author	Channel geometry, D_h	Relative roughness, k/D_h	Results	Remarks
Celata et al. [7]	Stainless steel and glass tubes (146–440 μm)	0.004–0.007 based on R_a	No effect of roughness	Drop in Nu for glass tubes due to conduction in the wall
Grohmann [8]	Microtubes (250–500 μm)	0.014–0.036 based on R_a	Continuous increase in Nu/Nu_{conv} for $Re < 700$	Cryogenic temperatures
Kandlikar et al. [9]	Stainless steel tubes (620–1067 μm)	0.0016–0.0036 based on R_a	No effect of roughness for $D_h = 1067$ μm; $Nu/Nu_{smooth} \approx 1.5$–$1.7$ for $D_h = 620$ μm and $k/D_h = 0.0036$	Slight increase in Nu for $Re = 1000$–2300
Li et al. [4]	Stainless steel tubes (300–1570 μm)	0.014–0.024	$Po/Po_{smooth} = 1.10$–1.16; No effect of roughness on Nu	Strong effect of axial conduction for low Re
Liu et al. [10]	Stainless steel tubes (168–399 μm)	0.027–0.035	Increase in Po for $Re > 1100$ and in Nu for $Re > 500$ Continuous increase in Nu. $Nu/Nu_{conv} \approx 1$ for $Re < 500$	Attributed to earlier transition
Qu et al. [11]	Trapezoidal microchannels (51–169 μm)	0.012–0.017 semi-rough channels (smooth cover plate)	$Po/Po_{smooth} = 1.08$–1.3. Po increases with Re. $Nu/Nu_{conv} \approx 0.25$–$0.5$	Definition of k not specified Roughness–viscosity model
Rahman [12]	Rectangular microchannel (≈ 300 μm)	Roughness not given	Increase in Nu with higher slope than for conventional channels. $Nu/Nu_{conv} \approx 1$ for $Re \approx 500$–700	Attributed to roughness
Shen et al. [13]	Rectangular microchannel (436 μm)	0.04–0.06	$Po/Po_{smooth} = 0.06Re^{0.53}$, $Nu/Nu_{conv} \approx 0.4$	Definition of k not specified
Wu and Cheng [14]	Trapezoidal microchannels (No. 9–10) (83–160 μm)	0.006–0.011 semi-rough channels (smooth cover plate)	$Po/Po_{smooth} = 1.06$–1.2, $Re = 100$–1000, $Nu/Nu_{smooth} \approx 1.2$–$1.4$	Developing flow, definition of k not specified Axial conduction

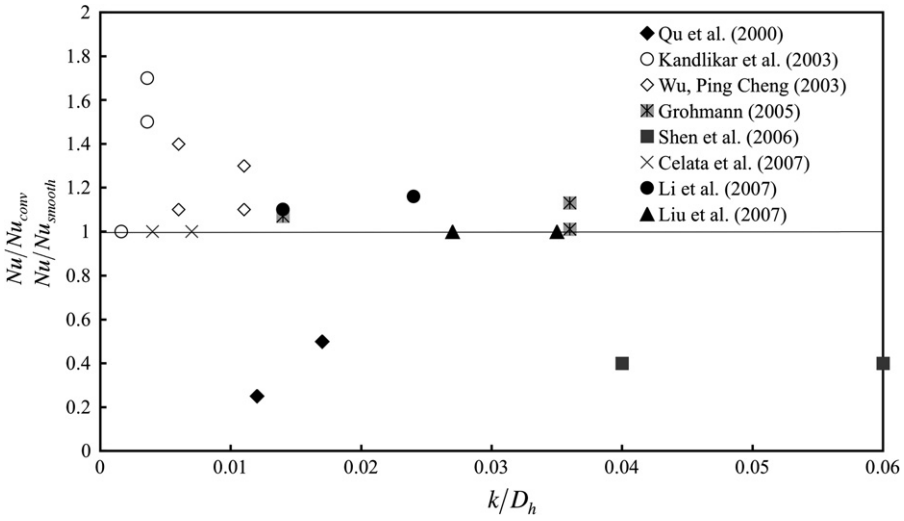

Fig. 1. Comparison of published experimental results on the Nusselt number for rough microchannels. Open symbols correspond to Nu/Nu_{smooth}; solid symbols correspond to Nu/Nu_{conv}.

may also be noticed that the roughness is rarely well characterized in these studies.

Various models have been proposed to account for roughness effects in laminar flows. Mala and Li [2] introduced a roughness viscosity model in order to interpret the increase in *Po* that they observed in their experiments. The increase of momentum transfer due to roughness was modelled by the addition of an empirical roughness viscosity to the fluid molecular viscosity: $\mu_{eff} = \mu + \mu_R$. Qu et al. [11] later used this roughness viscosity model for interpreting the small value of the Nusselt number that they observed in rough microchannels, when compared to Nu_{conv}.

Koo and Kleinstreuer [15] introduced the concept of an equivalent porous medium layer to model the rough near-wall region. They were able to predict the effects of the thermal conductivity ratio between the surface roughness layer and bulk fluid, the layer permeability, and relative surface roughness (0.01–0.04) on the Nusselt number [16]. They found an increase in Nu/Nu_{conv} up to 1.09 for flows between parallel plates, when the solid/fluid conductivity ratio and the porous layer permeability were sufficiently high. On the contrary, they found Nu/Nu_{conv} lower than 1 for small solid/fluid conductivity ratio and porous layer permeability.

Croce and co-authors [17–19] carried out numerical computations in microchannels with rough elements periodically distributed on a smooth surface heated at constant temperature. Croce and D'Agaro considered two-dimensional rectangular or triangular elements placed on the surface of a plane channel or a circular tube [17,18]. The relative roughness was in the range 0.005–0.053. The authors obtained a very large increase in *Po* ($\approx 100\%$) for the highest value of the relative roughness (0.053). On the other hand, they obtained an increase in Nu/Nu_{smooth} for a plane channel and a decrease of this quantity in a circular tube. They explained this behaviour as resulting from a balance between enhanced heat transfer in the region of peaks (top of the rough elements) and reduced heat transfer in the region of valleys (between the rough elements). More recently, Croce et al. [19] analysed the case of three-dimensional conical elements placed on the surface of a plane channel. A much weaker effect than for two-dimensional obstructions was obtained by the authors in this case, as expected. A correlation was proposed in [19] for *Po* and *Nu* as a function of the relative roughness and the geometric characteristics of the rough elements. In all of these computations, the Poiseuille number and the Nusselt number were found to be nearly independent of the Reynolds number. Andrade et al. [20] numerically investigated the effect of rough walls with a fractal geometry on the two-dimensional transport of heat through a plane channel. They found an enhancement of heat transfer only when the Peclet number was larger than about 800 ($Pe = RePr$, where *Pr* is the fluid Prandtl number). The authors, however, do not give the value of their roughness height. Zeng et al. [21] recently investigated the surface roughness effect on flow and mass transfer in the context of microchannel bioreactors. They considered two-dimensional semi-circle or triangle bulges also uniformly distributed on the bottom wall of a two-dimensional flat-plate and found a strong increase in the pressure gradient and a significant mixing enhancement for rough walls compared to smooth ones.

The above presentation shows that roughness effects on heat transfer in microchannel flows are so far not well characterized. There are few well-documented experimental studies on this subject. Roughness effects may be obscured by very large uncertainties in the measurements and other effects present in microchannel flows. Most numerical investigations consider two-dimensional bulges whereas the surface finish likely consists three-dimensional bumps in machined microchannels.

The current work is focused on heat transfer in fully-developed laminar flows through rough microchannels. It is the extension of a research project on the flows in rough microchannels. In this project, a test section with a three-dimensional periodic pattern of rough elements was built and tested. This geometry was chosen because it is easily obtained via deep reactive ion etching of silicon wafers [5]. Moreover, it enables both a very good control of the roughness structure in experimental test sections and a rather simple modelling of the flow and associated heat transfer. In fact, the surface texture of industrial microdevices is constituted by structures of different sizes and shapes depending on manufacturing processes. The present model may be considered as a first step to approach such a roughness structure. Additionally, the model is representative of a heat exchanger with pin fins for high values of the rough elements height.

A previous study [5] has shown that numerical three-dimensional computations and a one-dimensional model of the flow in microchannels with periodic rough elements are in good agreement with the experimental results. The same geometry was chosen in the present work to compute the heat transfer coefficient associated with the flow [22]. The three-dimensional numerical approach and the one-dimensional model used in our previous work were extended to the heat transfer problem. The objective of the present

paper is to highlight the relevant roughness parameters and to specify their influence on heat transfer in microchannels.

2. Geometrical model of roughness, flow and thermal conditions

In the present modelling investigation, the surface roughness consists of blocks periodically distributed on the plane walls of a microchannel of infinite span. The spacing between walls is denoted by H. The roughness elements are parallelepipeds of height k and square cross-section of side length d which are distributed either in aligned or staggered arrangements (Fig. 2). The distribution of roughness elements is identical on the two channel parallel walls. The x, y, z axes are aligned with the streamwise, normal and spanwise directions respectively. The origin is located on the reference surface at the bottom of the rough elements. The wavelength λ of the block pattern is the same in x and z directions ($\lambda = L$ or $2L$ for the aligned or staggered arrangements, respectively). The geometric description of the rough microchannel is characterized by the following three dimensionless numbers:

i) the relative roughness, here normalized with the half channel height,

$$k^* = \frac{k}{H/2} \tag{1}$$

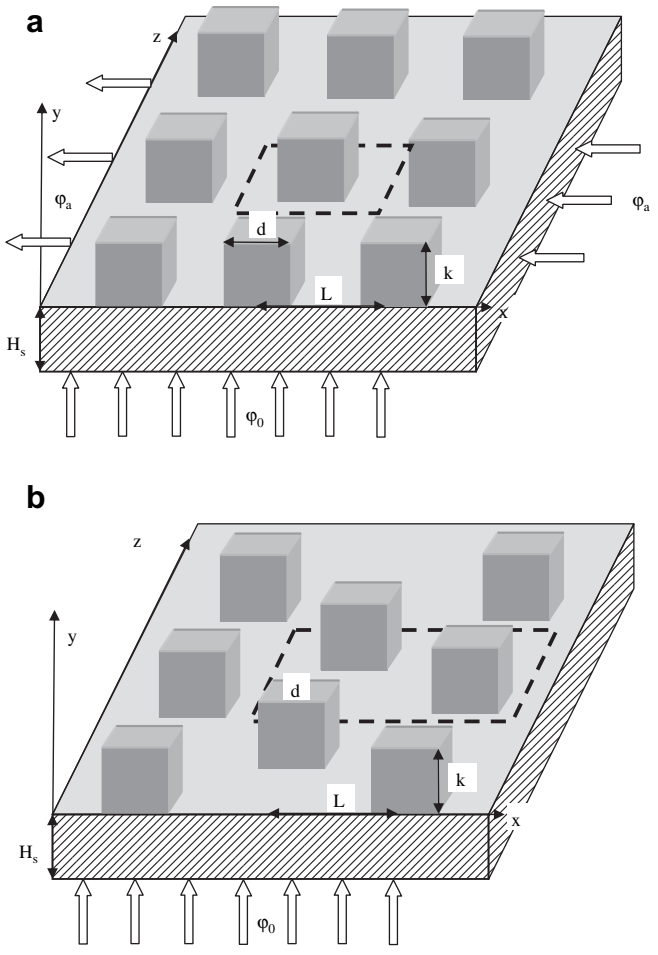

Fig. 2. Sketch of the rough elements. (a) Aligned arrangement; (b) staggered arrangement. Dashed lines show the base of the computational domain in the reference plane.

One may notice that k^* is four times larger than the usual relative roughness, normalized with the hydraulic diameter.

ii) the porosity ε reflects the compactness of the rough region and, according to its usual definition in porous media, is given by

$$\varepsilon = 1 - \frac{d^2}{L^2} \tag{2}$$

iii) a second local parameter is obtained from a combination of k, d, and L independently of Eq. (2). We chose the ratio k/L, which reflects the density of the rough elements in the pattern. Writing $\varepsilon = 1 - ((k/L)/(k/d))^2$, it is clear that the same porosity may be obtained with slender elements very close to each other (high k/L and k/d) or flat elements far from each other (small k/L and k/d). Alternatively, we also used

$$L^{*2} = \frac{L^2}{(H/2)^2} \tag{3}$$

which indicates the roughness structure fractionation ($F = 1/L^{*2}$ is the number of rough elements in a square of side $H/2$) with obvious relations between the various dimensionless parameters. It is worth emphasizing that the two parameters, ε and k/L, are intrinsic to the rough element pattern.

The flow is assumed to be laminar and fully-developed. We also assume that the fluid properties (density ρ_f, dynamic viscosity μ_f, specific heat at constant pressure C_{pf} and thermal conductivity k_f, Prandtl number Pr) are constant throughout the channel and that buoyancy is negligible. The flow is characterized by the bulk velocity $u_b = \dot{m}/\rho_f H$, where $\dot{m}$ is the mass flow rate per unit transverse length. The Reynolds number is based on the bulk velocity and the hydraulic diameter: $Re = 2\dot{m}/\mu_f$. The Poiseuille number is defined as

$$Po = -\frac{1}{\mu_f}\frac{dp}{dx}\frac{2\rho_f H^3}{\dot{m}} \tag{4}$$

where dp/dx is the pressure gradient across the microchannel. The rough elements of thermal conductivity k_s are placed on a substrate of thickness H_s and same conductivity. The substrate is heated with uniform heat-flux φ_0 at its rear side ($y = -H_s$). It is well known that axial conduction may take place in heated microchannels, in particular in the entrance region where the boundary layers are developing [23]. A thermally fully-developed region is, however, expected in sufficiently long channels and the present investigation is restricted to this region. As a result, the fluid temperature may be decomposed into a linear part and a periodic component like the pressure in the hydrodynamic problem [5,17]. The linear increase of the temperature is due to the uniform flux heating whereas the periodic variations result from the perturbations of the temperature field due to the rough elements. Temperatures are then functions of a slow variable X (the longitudinal abscissa of the order of the channel length) and fast variables (local coordinates of the order of λ). In the fluid, we may write

$$T(x,y,z) = \frac{dT_m(X)}{dX}X + \tilde{T}(x,y,z) \tag{5}$$

where $T_m(X)$ is the fluid bulk temperature and $\tilde{T}$ is periodic. The same hypothesis results in a similar decomposition of the solid temperature field

$$T(x,y,z) = \frac{dT_0(X)}{dX}X + \tilde{T}(x,y,z) \tag{6}$$

where $T_0(X)$ is the wall surface temperature associated with the slow variable. The assumption of a fully-developed thermal field leads to the same linear variation for $T_m(X)$ and $T_0(X)$.

Heat balance for a control volume delimited by a duct segment shows that the common temperature gradient along the channel is given by

$$\frac{dT_m}{dX} = \frac{dT_0}{dX} = \frac{2}{H}\frac{\varphi_0}{\rho_f C_{p_f} u_b} \tag{7}$$

A constant axial heat-flux φ_a across the wall section is related to the gradient dT_0/dX (Fig. 2).

$$\varphi_a = k_w \frac{2}{H}\frac{\varphi_0}{\rho_f C_{p_f} u_b} \tag{8}$$

The global Nusselt number is defined with the hydraulic diameter as

$$Nu = \frac{\varphi_0 2H}{k_f(T_0 - T_m)} \tag{9}$$

3. Numerical model

Three-dimensional computations were carried out using the geometrical model described in the previous section. The present numerical model follows the details of those developed successively by Hu et al. [24] and Bavière et al. [25] and includes an extension to the heat transfer problem.

The governing equations are

$$\nabla \vec{u} = 0 \tag{10}$$

$$\rho_f(\vec{u}\cdot\nabla\vec{u}) = -\nabla p + \mu_f \nabla^2 \vec{u} \tag{11}$$

$$\rho_f C_{p_f}(\vec{u}\cdot\nabla T) = k_f \nabla^2 T \tag{12}$$

for the fluid and

$$\nabla^2 T = 0 \tag{13}$$

for the solid. Because of the assumptions of constant fluid properties and negligible buoyancy, the mass and momentum equations are not coupled with the energy equation. Owing to periodicity, the computational domain extends over one wavelength in streamwise (x) and spanwise (z) directions and owing to symmetry, over the half channel height in the direction normal to the walls (y). The origin of the axes system is located at a distance $n\lambda$ from the channel entrance.

The dimensionless temperature is defined as

$$\theta(x,y,z) = \frac{T_0(X = n\lambda + x) - T(x,y,z)}{\varphi_0 D_h/k_f} \tag{14}$$

where $T_0(X)$ is the temperature of the reference surface ($y = 0$) associated with the slow variable. A periodic boundary condition is written for the velocity field and the reduced temperature (14) at the inlet and outlet sides of the computation domain.

$$\vec{u}(x+\lambda,y,z) = \vec{u}(x,y,z) \tag{15}$$

$$\theta(x+\lambda,y,z) = \theta(x,y,z) \tag{16}$$

Symmetry conditions are chosen at the lateral sides ($z = \pm\lambda/2$) and at the top of the computational domain ($y = H/2$) and the no-slip velocity condition at all the solid boundaries.

Numerical computations of the flow were carried out by using the commercial code Fluent 6.1.22. The equations were discretized by means of a finite volume method. A second-order upwind scheme was used for the advection terms whereas the diffusion terms were central-differenced. A SIMPLEC (Semi-Implicit Pressure Linked Equations Consistent) algorithm was used for the computations. Grid-convergence tests were carried out to verify the mesh accuracy. They were conducted with three grids having a number of mesh nodes equal to $32 \times 40 \times 32$, $48 \times 60 \times 48$, $64 \times 80 \times 64$ in the x, y, z directions respectively. The pressure gradient was chosen as the control parameter during the computations. The difference in the results as given by the coarse and the intermediate grids was 1.5%, and was 0.7% between the intermediate and the fine grids so that the grid $48 \times 60 \times 48$ was adopted for all the computations [25].

The computation time was about 4 h on a PC Pentium IV 2.4 GHz computer. The main results are presented later with those of the rough-layer model.

4. Rough-layer model

Koo and Kleinstreuer [15,16] proposed that the roughness region could be modelled as an equivalent porous medium layer adjacent to a clear fluid layer, namely the central part of the channel. They modelled the additional viscous forces due to rough elements in terms of the medium permeability and they used a non-linear term to account for inertia forces. Bavière et al. [25] used a discrete-element approach initially proposed by Taylor et al. [26,27] to compute the rough-wall skin friction and the heat transfer coefficient in turbulent flows. They developed an analytical one-dimensional model to compute the pressure drop in a microchannel. This model was extended by Gamrat et al. [5] into the rough-layer model (RLM hereafter), which combines ideas from the porous medium layer model of Koo and Kleinstreuer [15] and from the approach of Taylor et al. [26]. The authors improved the model of Bavière et al. [25] by refining both the interfacial condition between the rough-layer and the clear fluid layer and the modelling of the drag coefficient of the roughness elements. The RLM model is extended to heat transfer in this section.

4.1. Momentum equation

The method of volume averaging was applied to derive the macroscopic momentum equation in the rough-layer [26,27]. The approach considers a control volume (CV) of infinitesimal thickness δy in the direction normal to the wall (Fig. 3). Since the structures are periodic, the extension of the CV is limited to one wavelength λ in x and z directions ($\lambda = L$ or $2L$ for the aligned or staggered arrangements, respectively). A plane parallel to the wall determines the cross-section s ($=d^2$) on each rough element.

The flow is supposed to be fully-developed and is modelled as one-dimensional. Note that the porosity (Eq. (2)) is identical to the blockage factor, defined by Taylor et al. [26] as the ratio of area open for flow to the total area. In the volume averaging technique, two types of average velocity are commonly used like in porous media [28], namely the filtration or superficial averaged velocity $\langle u(y)\rangle$ and the effective or intrinsic averaged velocity $\langle u(y)\rangle^f$ in the fluid region which are related by

$$\langle u(y)\rangle = \varepsilon \langle u(y)\rangle^f \tag{17}$$

The filtration velocity $\langle u(y)\rangle$ is, however, more relevant than the effective velocity because it is representative of the mass flow rate. Then, the local Reynolds number is defined as

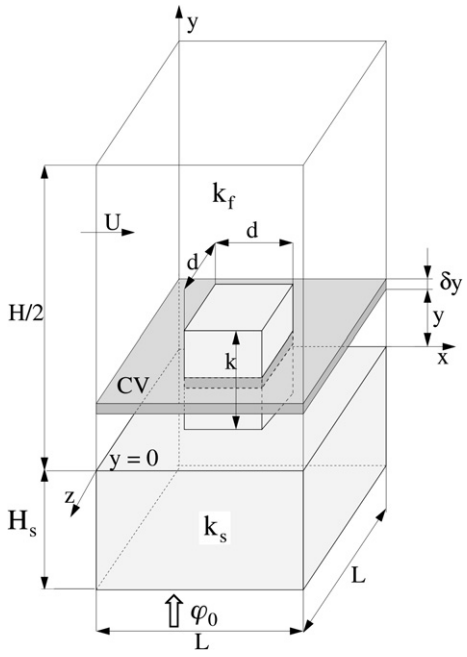

Fig. 3. Numerical model. Three-dimensional view of the computational domain.

$$Re_d(y) = \frac{\rho_f \langle u(y)\rangle d}{\mu_f} \tag{18}$$

The momentum equation for the CV results from the competition between the pressure forces acting on its upstream/downstream sides, the viscous shear stresses acting on its upper/lower sides and the drag force due to the rough element (for details, see Bavière et al. [25]). The dispersion term due to the spatial variations of the velocity components is neglected like in [16]. Periodicity allows decomposing the pressure into a linear part and a periodic component like in the work of Croce and D'Agaro [17],

$$p(x,y,z) = \frac{dp}{dx}X + \tilde{p}(x,y,z) \tag{19}$$

where X is the slow variable. Applying this pressure decomposition, one can separate the pressure forces into a contribution from the overall pressure gradient and from the periodic part $\tilde{p}$. Considering this latter one, the drag force due to the portion of rough element included in the CV is modelled by using a drag coefficient C_d

$$\delta F_d(y) = \frac{1}{2}\mu_f Re_d(y) C_d(y) \langle u(y)\rangle \, \delta y \tag{20}$$

$C_d(y)$ is the sum of two terms:

- the pressure coefficient related to the periodical pressure forces acting on the front and rear sides of the rough element, $C_{dp} = \Delta\tilde{p}/(1/2\rho_f\langle u\rangle^2)$, where $\Delta\tilde{p}$ is the averaged pressure difference between these two sides;
- the friction factor related to the friction forces, $C_{df} = 2\tau/(1/2\rho_f\langle u\rangle^2)$ where τ is the averaged wall shear stress on the lateral sides of the rough element.

The drag force due to the pressure gradient component is regrouped with the pressure term in the momentum equation

$$-\varepsilon\frac{dp}{dx} - \frac{1}{2L^2}\mu_f Re_d(y) C_d(y) \langle u(y)\rangle + \mu_f \frac{d^2\langle u(y)\rangle}{dy^2} = 0 \tag{21}$$

This equation has to merge with the momentum equation written for the clear region

$$-\frac{dp}{dx} + \mu_f \frac{d^2\langle u(y)\rangle}{dy^2} = 0 \tag{22}$$

4.2. Energy equation

We use a two-equation model for computing heat transfer. The thermal field is described in this one-dimensional model by the superficial averaged temperatures $\langle T_f(y)\rangle, \langle T_s(y)\rangle$ for the fluid and the solid respectively and the intrinsic averaged temperatures $\langle T_f(y)\rangle^f$, $\langle T_s(y)\rangle^s$ in the fluid and solid regions respectively. They are related by

$$\langle T_f(y)\rangle = \varepsilon \langle T_f(y)\rangle^f \tag{23}$$

$$\langle T_s(y)\rangle = (1-\varepsilon)\langle T_s(y)\rangle^s \tag{24}$$

The energy budget for the CV defined in the previous section results from the balance between longitudinal advection by the flow and conduction through the fluid and the solid in the transverse direction. The thermal dispersion term has been neglected like in the momentum equation.

$$-\rho_f C_{p_f} \langle u\rangle \frac{dT_m}{dx} + k_s \frac{d^2\langle T_s(y)\rangle}{dy^2} + k_f \frac{d^2\langle T_f(y)\rangle}{dy^2} = 0 \tag{25}$$

This equation is complemented by the energy equation inside the solid part CV_s of the control volume CV

$$k_s \frac{d^2\langle T_s(y)\rangle^s}{dy^2} = \varphi(y)\frac{4}{d} \tag{26}$$

where $\varphi(y)$ is the heat-flux exchanged by CV_s with the stream.

Substituting the left-hand term of Eq. (26) into Eq. (25), using Eq. (7) and eliminating $\langle T_f\rangle$ results in

$$k_f \frac{d^2\langle T(y)\rangle}{dy^2} = \frac{\langle u(y)\rangle}{u_b}\frac{2\varphi_0}{H} - \varphi(y)\frac{4d}{L^2}\left(1-\frac{1}{\Lambda}\right) \tag{27}$$

where Λ is the ratio of solid to fluid conductivity. The superficial averaged temperature $\langle T(y)\rangle$ is the sum of the corresponding fluid/solid temperatures

$$\langle T(y)\rangle = \langle T_f(y)\rangle + \langle T_s(y)\rangle \tag{28}$$

We could also have introduced the averaged enthalpic temperature defined with the superficial fluid/solid temperatures weighted by the volumetric heat capacity of the two phases respectively. Although this definition has a better physical meaning, it leads to a more complicated formalism and has not be retained in this work.

From the point of view of the discrete-element approach [27], the heat-flux $\varphi(y)$ may be expressed using a local Nusselt number

$$Nu_d(y) = \frac{\varphi(y)d}{k_f\left[\langle T_s(y)\rangle^s - \langle T(y)\rangle\right]} \tag{29}$$

The two-equation model is finally defined by the following equations:

$$\frac{d^2\langle T(y)\rangle}{dy^2} = \frac{\langle u(y)\rangle}{u_b}\frac{2\varphi_0}{k_f H} - Nu_d(y)\frac{4\left[\langle T_s(y)\rangle^s - \langle T(y)\rangle\right]}{L^2}\left(1-\frac{1}{\Lambda}\right) \tag{30}$$

$$\Lambda\frac{d^2\langle T_s(y)\rangle^s}{dy^2} = Nu_d(y)\frac{4\left[\langle T_s(y)\rangle^s - \langle T(y)\rangle\right]}{d^2} \tag{31}$$

4.3. Drag coefficient and heat transfer coefficient modelling

In this model, Koo and Kleinstreuer [15] introduced an ad hoc value of the permeability in order to fit the experimental results of Guo and Li [29]. In the discrete-element model, Taylor et al. [26,27] introduced empirical correlations for the drag force and the heat transfer coefficients. These expressions, however, relate the two coefficients to the local Reynolds number only and ignore other geometrical parameters like the distance between rough elements. The current investigation used two-dimensional numerical simulations for the purpose to better estimate these coefficients.

In a first step, the three-dimensional numerical simulations described in Section 3 were used to compute the distribution of the drag coefficient $C_d(y)$ and the local Nusselt number $Nu_d(y)$ along a parallelepipedic roughness element as a function of the local Reynolds number for several values of the geometrical parameters. Results [5] (not shown here) clearly demonstrate that the drag coefficient C_d is inversely proportional to Re_d. The proportionality factor C_r ($C_r = C_d Re_d$, resistance coefficient hereafter) varies with neither the global Reynolds number Re nor the relative roughness height k^* and mainly depends on the porosity ε. It is worth emphasizing that this advantage results from applying the pressure decomposition as given by Eq. (18). The overall pressure gradient is strongly dependent on the global structure of the microchannel characterized by the relative roughness whereas the drag coefficient C_d is directly dependent on the local velocity field and the local geometrical structure of roughness. The local Nusselt number is also strongly influenced by the porosity, as expected (Fig. 4). Each series of points in Fig. 4 was obtained by varying the position y along a roughness element while keeping constant the geometric parameters and the global Reynolds number. Note that the abscissa Re_d is proportional to the local superficial velocity and is therefore an ascending function of y. For low values of Re_d (<1), the figure reveals that there is a rather satisfying overlap between the results obtained with varying k^* and F, ε being kept constant ($=0.75$). End effects are, however, present in the distribution of Nu_d along a rough element. In particular, each series of points present an abrupt increase in Nu_d for the highest values of Re_d, corresponding to the top of the roughness elements. This is most probably due to the three-dimensional effect of the velocity and thermal field in this region. Another three-dimensional effect is also present, especially for $Re = 200$, at the bottom of the rough elements, where an increase in Nu_d is observed when Re_d is decreased, namely towards the reference surface. This is due to the complex interactions between convection and conduction in the solid/fluid parts of the rough region near the reference surface. Similar, but weaker end effects were also observed for the resistance coefficient C_r [5].

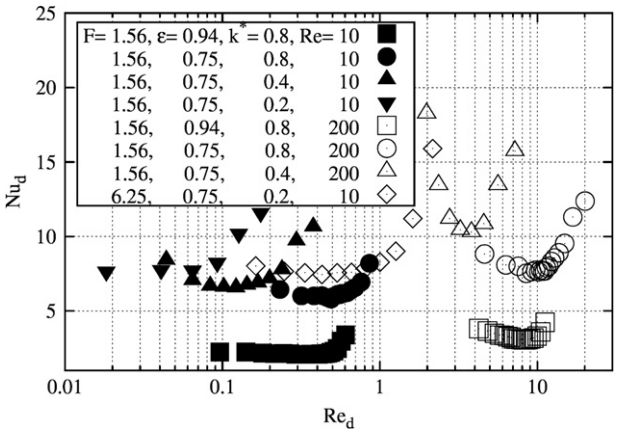

Fig. 4. Variations of the local Nusselt number Nu_d along the roughness elements. Results of the three-dimensional simulations. $Pr = 7$. $\Lambda = 195$.

Despite this presence of end effects, the heat transfer coefficient was modelled like the drag coefficient by means of two-dimensional numerical simulations of the flow across a bank of rods instead of computationally expensive three-dimensional simulations. These computations were carried out by Gamrat et al. [30] for the aligned and staggered arrangements of rods with square cross-section. A condition of constant volumetric heat source in the rods was used in their work. The following correlations were obtained from their results by using a least-square method:

$$C_r = \left[a_1(1-\varepsilon)^{n_1}\exp(b_1(1-\varepsilon))\right] + \left[a_2(1-\varepsilon)^{n_2}\exp(b_2(1-\varepsilon))\right]Re_d \tag{32}$$

with $a_1 = 52.2$, $b_1 = 4.5$, $n_1 = 0.27$, $a_2 = 0.15$, $b_2 = 2.13$, $n_2 = -0.23$ in the aligned arrangement; $a_1 = 62.2$, $b_1 = 4.64$, $n_1 = 0.28$, $a_2 = 6.4$, $b_2 = 0.9$, $n_2 = -0.4$ in the staggered arrangement.

The pressure coefficient C_{dp} and the friction factor C_{df} were distinguished. It was found that C_{df} contributes by 50% ($\pm 5\%$) to the total drag coefficient. For heat transfer, the authors found

$$Nu_d = \left[a_3(1-\varepsilon)^{n_3}\exp(b_3(1-\varepsilon))\right] + [a_4(1-\varepsilon)+c]{Re_d}^{0.5}Pr^{0.2} \tag{33}$$

with $a_3 = 3.02$, $b_3 = 2.54$, $n_3 = 0.278$; $a_4 = 0.44$, $c = 0.092$ in the aligned arrangement; $a_4 = 1.093$, $c = 0.357$ in the staggered arrangement.

4.4. Boundary conditions and dimensionless equations

After volume averaging, the problem of fluid flow in rough-wall microchannels reduces to a second-order ordinary differential equation. The system of equations (21), (30,31) can be solved numerically under appropriate boundary conditions. It was assumed that the velocity is equal to zero at the bottom wall ($y = 0$) whereas symmetry boundary conditions were used at the channel plane of symmetry ($y = 0.5H$). The formulation of the boundary conditions at a homogeneous fluid/porous layer interface has been analysed by several authors. The survey study of Alzami and Vafai [31] can be used as a reference on this subject. The continuity of filtration velocity $\langle u \rangle$ is satisfied in the whole computational domain. For the discrete-element approach, a particular problem arises when cylindrical or prismatic elements are considered. Bavière et al. [25] assumed the continuity of the effective velocity gradient at the clear fluid/porous layer interface. A discontinuity of the effective velocity gradient is, however, expected at the interface owing to the development of velocity boundary layers on the rough elements top surface. In order to account for this discontinuity, the RLM model [5] considers a control volume CV_N adjacent to the top of the rough elements. CV_N is defined with the same extension as CV (Fig. 3) in x and z directions and by $k \le y \le k + \delta y$. The force induced by the rough element on CV_N is restricted to the viscous force at its top horizontal surface. The model assumes that the boundary layers developing on the top surface and the lateral sides in the top part of the rough element are similar. As a consequence, the shear stress at the rough element top surface can be deduced from the average friction coefficient C_{df} on the lateral sides of the rough element. As explained before, this friction factor is deduced from the two-dimensional simulations, like the average drag coefficient C_d.

Similarly, the thermal boundary condition at the clear fluid/porous layer interface is replaced by the heat balance of CV_N,

$$\frac{d^2\langle T(y)\rangle}{dy^2}L^2\,\delta y = \frac{\langle u(y)\rangle}{u_b}\frac{2\varphi_0}{k_f H}L^2\,\delta y - Nu_N\left[\langle T_s(y)\rangle^s - \langle T(y)\rangle\right]\left(1-\frac{1}{\Lambda}\right)d \tag{34}$$

where Nu_N is defined with the heat-flux φ_{top} at the top surface of a rough element as

$$Nu_N = \frac{\varphi_{top} d}{k_f\left[\langle T_s(k)\rangle^s - \langle T(k)\rangle\right]} \tag{35}$$

The present model assumes that the Nusselt number Nu_N at the top surface of CV_N is identical to that of the lateral sides (planes parallel to xy) of a rough element, denoted by Nu_{lat}. The two-dimensional simulations [30] have shown that

$$Nu_{lat} \approx Nu_d \quad \text{for the staggered arrangement} \tag{36}$$

$$Nu_{lat} \approx (2.15-\varepsilon)Nu_d \quad \text{for the aligned arrangement}$$

and

$$5 < Re_d < 40,\ \ 0.44 < \varepsilon < 0.98 \tag{37}$$

where Nu_d is given by Eq. (33).

Finally, the system of dimensionless equations for the flow field is the following:

$$0 \le y^* \le k^* \quad 0 = \frac{\varepsilon Po}{8} - C_r\frac{\langle u\rangle^*}{2L^{*2}} + \frac{d^2\langle u\rangle^*}{dy^{*2}} \tag{38}$$

$$k^* \le y^* \le k^* + \delta y^* \quad 0 = \frac{Po}{8} - C_{df}Re_d\frac{\langle u\rangle^*}{2L^{*2}}\frac{d^*}{2\delta y^*} + \frac{d^2\langle u\rangle^*}{dy^{*2}} \tag{39}$$

$$k^* + \delta y^* \le y^* \le 1 \quad 0 = \frac{Po}{8} + \frac{d^2u^*}{dy^{*2}} \tag{40}$$

where the lengths and velocities are normalized by $H/2$ and the bulk velocity u_b respectively and are denoted by the superscript $()^*$. C_r and C_{df} are deduced from Eq. (32). The presence of δy^* in the second term of Eq. (39) is due to the fact that the resulting pressure force and viscous force in the momentum equation are proportional to δy^* whereas the viscous force on the top surface of the rough element does not depend explicitly on δy^*. Contrary to the case of Eq. (38), the slide height of the control volume does not eliminate in the momentum equation applied to CV_N leading to Eq. (39).

For heat transfer, the system of equations is the following:

$$0 \le y^* \le k^* \quad \frac{d^2\langle\theta\rangle}{dy^{*2}} = \frac{\langle u^*\rangle}{4} - Nu_d\left(\langle\theta_s\rangle^s - \langle\theta\rangle\right)\frac{4}{L^{*2}}\left(1-\frac{1}{\Lambda}\right) \tag{41}$$

$$\frac{d^2\langle\theta_s\rangle^s}{dy^{*2}} = Nu_d\left(\langle\theta_s\rangle^s - \langle\theta\rangle\right)\frac{1}{L^{*2}(1-\varepsilon)\Lambda} \tag{42}$$

$$k^* \le y^* \le k^* + \delta y^* \quad \frac{d^2\langle\theta\rangle}{dy^{*2}} = \frac{\langle u^*\rangle}{4} - Nu_N\left(\langle\theta_s\rangle^s - \langle\theta\rangle\right)\frac{1}{L^{*2}}\left(1-\frac{1}{\Lambda}\right)\frac{d^*}{\delta y^*} \tag{43}$$

$$k^* + \delta y^* \le y^* \le 1 \quad \frac{d^2\langle\theta\rangle}{dy^{*2}} = \frac{\langle u^*\rangle}{4} \tag{44}$$

Eqs. (41) and (42) correspond to the fluid and the solid parts of the rough-layer respectively. The two systems of equations are complemented by the following boundary conditions:

For the flow field

$$y^* = 0 \quad \langle u\rangle^* = 0 \tag{45}$$

$$y^* = k^* \quad \langle u\rangle^*\left(k^{*-}\right) = \langle u\rangle^*\left(k^{*+}\right) \tag{46}$$

$$y^* = k^* \quad \left.\frac{d\langle u\rangle^*}{dy}\right|_{k^*|-} = \left.\frac{d\langle u\rangle^*}{dy}\right|_{k^*|+} \tag{47}$$

$$y^* = k^* + \delta y^* \quad \langle u\rangle^*\left(k^* + \delta y^*\big|^-\right) = \langle u\rangle^*\left(k^* + \delta y^*\big|^+\right) \tag{48}$$

$$y^* = k^* + \delta y^* \quad \left.\frac{d\langle u\rangle^*}{dy}\right|_{k^*+\delta y^*|-} = \left.\frac{d\langle u\rangle^*}{dy}\right|_{k^*+\delta y^*|+} \tag{49}$$

$$y^* = 1 \quad \frac{du^*}{dy^*} = 0 \tag{50}$$

For the thermal field, the dimensionless temperature θ is defined by Eq. (14)

$$y^* = 0 \quad \langle\theta\rangle = 0 \quad \langle\theta_s\rangle^s = 0 \tag{51}$$

$$y^* = k^* \quad \langle\theta\rangle\left(k^{*-}\right) = \langle\theta\rangle\left(k^{*+}\right) \tag{52}$$

$$y^* = k^* \quad \left.\frac{d\langle\theta\rangle}{dy}\right|_{k^*|-} = \left.\frac{d\langle\theta\rangle}{dy}\right|_{k^*|+} \quad \frac{d\langle\theta_s\rangle^s}{dy^*} = \frac{1}{\Lambda}\frac{Nu_N\left(\langle\theta_s\rangle^s - \langle\theta\rangle\right)}{d^*} \tag{53}$$

$$y^* = k^* + \delta y^* \quad \langle\theta\rangle\left(k^* + \delta y^*\big|^-\right) = \langle\theta\rangle\left(k^* + \delta y^*\big|^+\right) \tag{54}$$

$$y^* = k^* + \delta y^* \quad \left.\frac{d\langle\theta\rangle}{dy}\right|_{k^*+\delta y^*|-} = \left.\frac{d\langle\theta\rangle}{dy}\right|_{k^*+\delta y^*|+} \tag{55}$$

$$y^* = 1 \quad \frac{d\theta}{dy^*} = 0 \tag{56}$$

The solution of systems (38)–(40) depends on the three dimensionless geometrical parameters already defined: the relative roughness height k^*, the porosity ε of the roughness region and the roughness structure fractionation ratio $F = 1/L^{*2}$. It may be remarked that the term of interaction between the flow and the rough elements is inversely proportional to L^{*2} so that a high degree of fractionation of the rough elements for a given porosity is related to a high resistance of the rough-layer to the flow. The solution of systems (41)–(44) explicitly depends on the three previous parameters and additionally on the conductivity ratio $\Lambda = k_s/k_f$. It also depends implicitly on the Prandtl number, which influences the local Nusselt number (Eq. (33)).

The two systems of equations were discretized and solved by means of a first order finite difference method using the software Matlab. Due to the strong variations of velocity in the normal direction, the rough-layer was typically discretized in about 100 slices and the extra layer ($k^* \le y^* \le k^* + \delta y^*$) in 5 slices. The RLM model was applied to a laminar flow with $Pr = 7$. The influence of the thickness δy of the CV_N was found to be negligible on the

numerical results. In fact, the Poiseuille number varied by ±1% when the normalized thickness δy^* was changed from 0.002 to 0.02. The computation time was less than 10 s on a PC Pentium IV 2.4 GHz computer.

5. Results

The three-dimensional computations have shown that the Poiseuille number Po is nearly independent of Re and that the global Nusselt number Nu slightly increases with Re [22], confirming the results of Croce et al. [19] and our previous experiments (for Po). More precisely, Po/Po_{smooth} increases from 1.593 to 1.6 when Re increases from 10 to 200 and for the following typical set of parameters: $\varepsilon = 0.75$, $F = 1.56$, $k^* = 0.2$. Nu/Nu_{smooth} increases from 1.29 to 1.34 for the same increase in Re and for $\varepsilon = 0.75$, $F = 1.56$, $k^* = 0.24$. The staggered and aligned arrangements gave almost identical results for the friction factor and the heat transfer coefficient. The maximum difference between the results for the two arrangements was found to be equal to 5% for small values of the parameter F (flat roughness elements). The following results were obtained with $Pr = 7$ and $\Lambda = 195$, simulating a flow of water in a microchannel with silicon walls.

5.1. Velocity and temperature profiles

Fig. 5 shows velocity and temperature profiles obtained with the RLM model and the three-dimensional numerical simulations at constant mass flow rate for two different values of the relative rough elements height k^* while the porosity and L^{*2} were kept constant. The profiles provided by the numerical simulations were averaged over one wavelength in the x and z directions, for sake of comparison with the RLM results. The Poiseuille profile and the theoretical temperature profile for a flow between smooth parallel plates are also shown for comparison. As expected, the velocity is strongly reduced in the rough-layer, where the velocity profiles exhibit a nearly linear variation for this choice of parameters. The temperature profile in the solid phase is very flat due to the high conductivity of silicon. The observed differences between fluid and solid temperatures indicate that the assumption of thermal equilibrium is not appropriate in the present case. Fig. 5 shows an excellent agreement between the two approaches used in the present work.

5.2. Friction factor and heat transfer coefficient

The Poiseuille number and the global Nusselt number are normalized by the corresponding values of the smooth case ($Po_{smooth} = 24$, $Nu_{smooth} = 8.235$) and plotted as a function of k^* for three different values of the porosity in Fig. 6. On the same figure, we have plotted Po_{max}/Po_{smooth} and Nu_{max}/Nu_{smooth} which correspond to the Poiseuille flow computed with the reduced flow passage $H - 2k$ ($Po_{max}/Po_{smooth} = 1/(1-k^*)^3$, $Nu_{max}/Nu_{smooth} = 1/(1-k^*)$). The RLM model and the three-dimensional numerical simulations are again in excellent agreement to show a regular increase of Po and Nu with k^*, confirming the consistency of the RLM model with the other approach. As expected, smaller values of porosity cause higher increase in Po and Nu. It is worth noting that Po is very close to the maximum value Po_{max} for $\varepsilon = 0.44$. When compared to the numerical simulations, the RLM model slightly overpredicts the friction factor in this case.

The RLM's results are presented below by using an effective roughness height k_{eff}, or equivalently, a penetration depth $(k - k_{eff})$ of the driving shear into the rough-layer like in the analysis of Stroock et al. [32] of the flow over a two-dimensional sinusoidally modulated surface. This presentation has the advantage to relate

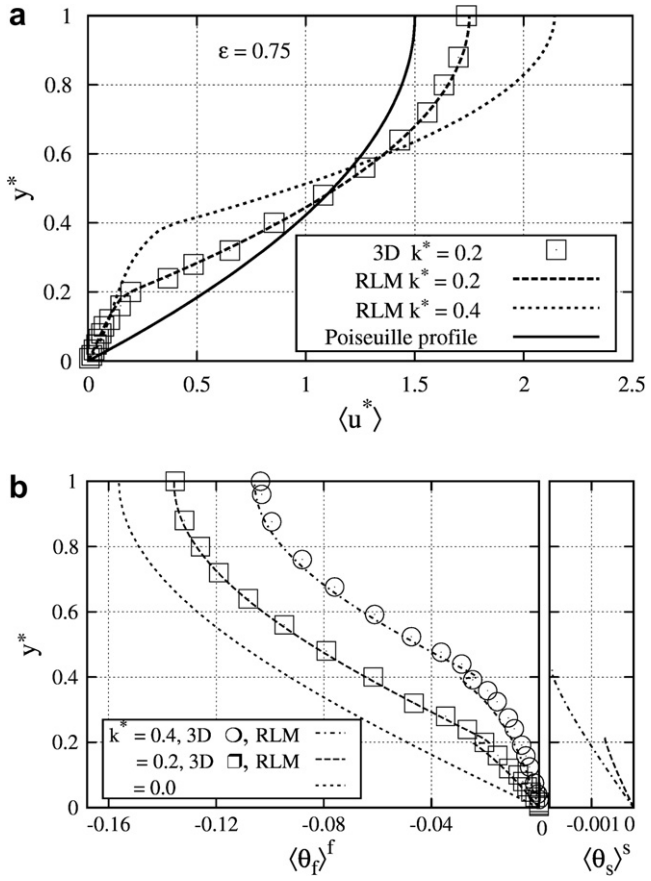

Fig. 5. Dimensionless profiles obtained at constant mass flow rate. $\varepsilon = 0.75$, $F = 1.56$, $Re = 200$, $Pr = 7$, $\Lambda = 195$. Aligned arrangement. Continuous lines: RLM model, symbols: 3D simulations; (a) superficial velocity profiles; (b) fluid and solid intrinsic temperatures. The scale is magnified 16 times for the solid phase temperature.

the roughness effects to the local geometric properties of the wall surface. For given flow rate, k_{eff} defines the location of the flat surface where the no-slip condition has to be satisfied by the Stokes flow in order to give the same Po as the actual rough-wall flow. Using Eq. (4), this definition corresponds to

$$\frac{k_{eff}}{k} = \left[1 - \left(\frac{Po_{smooth}}{Po}\right)^{1/3}\right]\frac{1}{k^*} \tag{57}$$

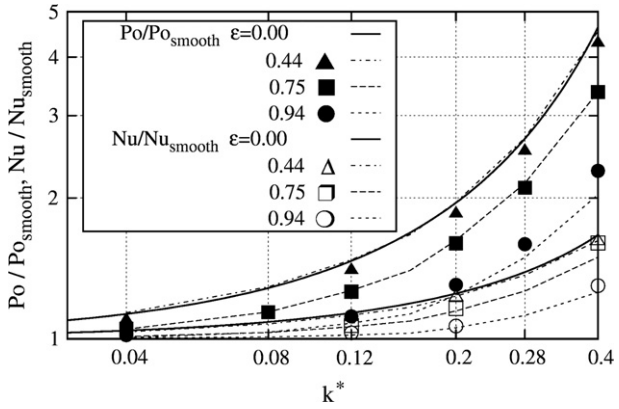

Fig. 6. Increase of Po and Nu with the relative roughness height. $F = 1.56$, $Re = 200$, $Pr = 7$, $\Lambda = 195$. Aligned arrangement. Continuous lines: RLM model; symbols: 3D simulations. $\varepsilon = 0$ corresponds to Po_{max}/Po_{smooth} and Nu_{max}/Nu_{smooth}.

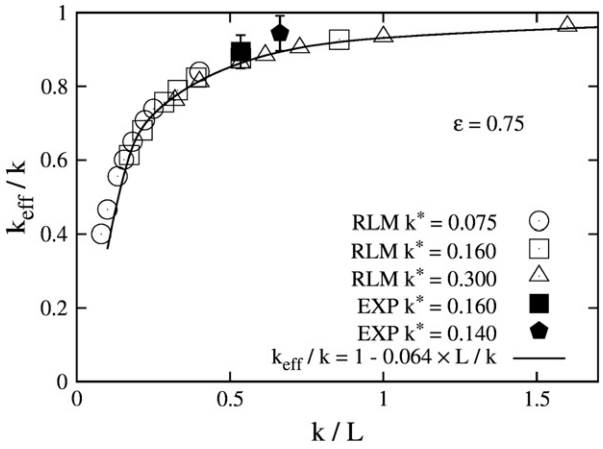

Fig. 7. Effective roughness height. Comparison between the rough-layer model and the analysis of Stroock et al. [32]. Staggered arrangement.

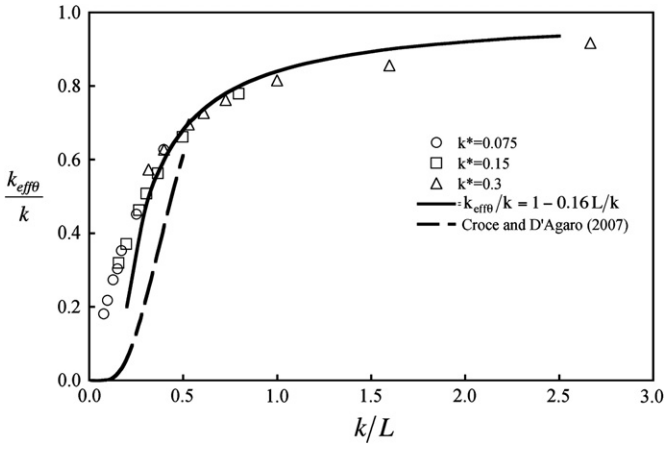

Fig. 9. Effective roughness height for heat transfer. $Pr = 7$, $\Lambda = 195$. Staggered arrangement.

An increase in k_{eff}/k obviously reflects an increase in Po. The normalized effective roughness height k_{eff}/k is plotted as a function of the local parameter k/L in Fig. 7, which shows that the results collapse on a single curve when the relative roughness k^* is varied, ε being kept constant. Moreover, the results are in good agreement with experimental results [5] plotted on the same graph. Using the asymptotic trends indicated by Stroock et al. [32] for small amplitude modulation of the wall, we find that the present results are well approximated by the law

$$\frac{k_{\text{eff}}}{k} = 1 - \frac{c(\varepsilon)}{2\pi}\frac{L}{k} \quad \text{for } \frac{k}{L} > 0.2 \tag{58}$$

with $c = 0.56$ for $\varepsilon = 0.75$.

For a first reasonable estimate of roughness effect, several authors have suggested to use a restricted hydraulic diameter $D_{h_{\text{app}}}$ computed with an apparent roughness height k_{app}, related in a simplified way to the structure of the rough-layer. For a two-dimensional channel flow, $D_{h_{\text{app}}} = 2(H - 2k_{\text{app}})$. In our geometric roughness model, the restricted hydraulic diameter may be estimated with the maximum roughness height ($k_{\text{app}} = k$) or with the porosity-weighted average between peaks and valleys ($k_{\text{app}} = k(1-\varepsilon)$). A simple average between peaks and valleys ($k_{\text{app}} = k/2$) may also be tested. These various estimates of the hydraulic diameter predict an increase in the Poiseuille number as given by

$$\frac{Po_{\text{app}}}{Po_{\text{smooth}}} = \frac{1}{\left(1 - \frac{k_{\text{app}}}{k}k^*\right)^3} \tag{59}$$

whereas the RLM model prediction is

$$\frac{Po}{Po_{\text{smooth}}} = \frac{1}{\left(1 - \frac{k_{\text{eff}}}{k}k^*\right)^3} \tag{60}$$

where k_{eff}/k is plotted in Fig. 7 for $\varepsilon = 0.75$. The comparison of the two approaches obviously depends on the rough-layer compactness. Considering one typical value of the porosity ($\varepsilon = 0.75$), and squared rough elements ($k/d = 1$), the corresponding value of the parameter k/L is 0.5 and the RLM model gives $k_{\text{eff}}/k = 0.87$. Fig. 8 and Table 2 compare the increase in Po as given by the various models. For this typical set of parameters, the best approximation relative to the RLM model is obtained with the maximum roughness height, which slightly overestimates the increase in the Poiseuille number. The porosity-weighted averaged roughness strongly underestimates the roughness effect. Although the simple average $k_{\text{app}} = k/2$ gives better results, it also underestimates the roughness effect. Similar trends are observed for a less compact rough-layer ($k/L = 0.21$, $k_{\text{eff}}/k = 0.7$), as shown by Fig. 8 and Table 2. In this case, however, the approximation of the roughness effect by $k_{\text{app}} = k$ significantly deteriorates whereas the prediction of Po by the model using the average $k_{\text{app}} = k/2$ slightly improves.

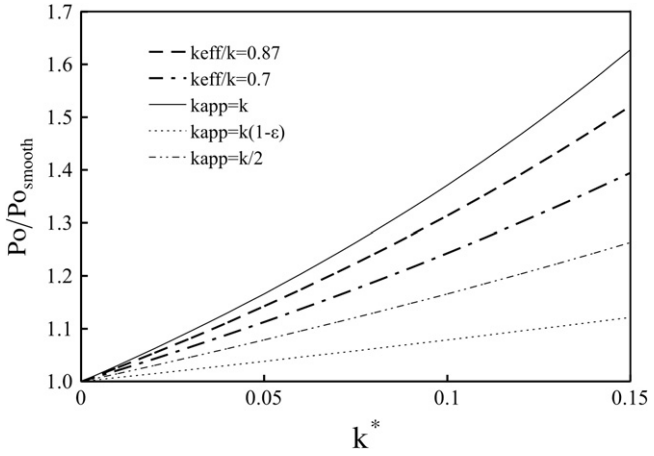

Fig. 8. Increase of Po with the relative roughness height. Comparison between approximate models of hydraulic diameter and the rough-layer model. $\varepsilon = 0.75$. Staggered arrangement.

In the same way as for the flow hydrodynamics, we define the effective thermal roughness height $k_{\text{eff}\theta}$, which gives the same heat-flux as the actual rough wall for a given temperature difference $T_0 - T_m$ and for the Stokes flow with zero velocity at $y = k_{\text{eff}\theta}$. This definition is equivalent to

$$\frac{k_{\text{eff}\theta}}{k} = \left(1 - \frac{Nu_{\text{smooth}}}{Nu}\right)\frac{1}{k^*} \tag{61}$$

The interpretation of $k_{\text{eff}\theta}$ is not fully correct from a physical point of view since the position of the virtual wall for the no-slip condition is actually for $y = k_{\text{eff}}$, which is different from $k_{\text{eff}\theta}$, as will be seen below. The same observation as for k_{eff} can be made for the effective thermal roughness height (Figs. 8 and 9), namely the results collapse on a single curve when the relative roughness k^* is varied, for $\varepsilon = 0.75$. The heat transfer results are well approximated by the law

Table 2
Relative increase in *Po* and *Nu*. Comparison between approximate models of hydraulic diameter and the rough-layer model. $\varepsilon = 0.75$.

		$k_{app} = k$	$k_{app} = k(1-\varepsilon)$	$k_{app} = k/2$
$(((Po_{app}/Po_{smooth}) - 1) - ((Po_{RLM}/Po_{smooth}) - 1))/((Po_{RLM}/Po_{smooth}) - 1)$	$k_{eff}/k = 0.87$	+15–20%	$\approx -75\%$	$\approx -45\%$
	$k_{eff}/k = 0.7$	+45–60%	$\approx -65\%$	$\approx -30\%$
$(((Nu_{app}/Nu_{smooth}) - 1) - ((Nu_{RLM}/Nu_{smooth}) - 1))/((Nu_{RLM}/Nu_{smooth}) - 1)$	$k_{eff\theta}/k = 0.66$	$\approx$+55%	$\approx -63\%$	$\approx -25\%$
	$k_{eff\theta}/k = 0.3$	$\approx$+250%	$\approx -17\%$	$\approx +70\%$

$$\frac{k_{eff\theta}}{k} = 1 - \frac{c_\theta(\varepsilon)}{2\pi}\frac{L}{k} \quad \text{for } \frac{k}{L} > 0.3 \tag{62}$$

with $c_\theta = 1.0$ for $\varepsilon = 0.75$. The comparison between Eqs. (58) and (62) shows that $k_{eff\theta} < k_{eff}$. This means that the roughness elements increase the friction factor more than the heat transfer coefficient for the conditions of this study. Croce et al. [19] proposed correlations for the Poiseuille and the Nusselt numbers as a function of the geometric characteristics of conical rough elements. The porosity is a function of the distance to the wall for this geometry. We used a mean porosity corresponding to the half-height of the conical elements in order to compare the present model to the authors' results. Fig. 9 shows that the two models are in consistency since a weaker heat transfer is expected for conical elements when compared to parallelepipedic ones.

The various models defining a restricted diameter may also be tested for the prediction of heat transfer. The trends are globally the same as for the flow hydrodynamics. However, since the roughness effect is less than for the friction factor, it is observed (Table 2) that the model using the maximum roughness height strongly overestimates the Nusselt number for $k/L = 0.5$ ($k_{eff\theta}/k = 0.66$). Contrary to the conclusions drawn for the Poiseuille number, the best estimate of the hydraulic diameter is the simple averaged roughness model ($k_{app} = k/2$) for $k_{eff\theta}/k = 0.66$ and the porosity-weighted averaged roughness model for $k/L = 0.13$ ($k_{eff\theta}/k = 0.3$) for predicting the Nusselt number.

5.3. Performance evaluation criteria

From an economical point of view, the interest of using a rough microchannel is evaluated by the performance evaluation criteria (PEC hereafter), defined by Webb [33], which compares the rough and the smooth cases.

$$\text{PEC} = \frac{j/j_{smooth}}{(f/f_{smooth})^{1/3}} = \frac{Nu/Nu_{smooth}}{(Po/Po_{smooth})^{1/3}} \tag{63}$$

where $j = Nu/(RePr^{1/3})$. Using Eqs. (57) and (61), PEC is also related to the effective passage heights by

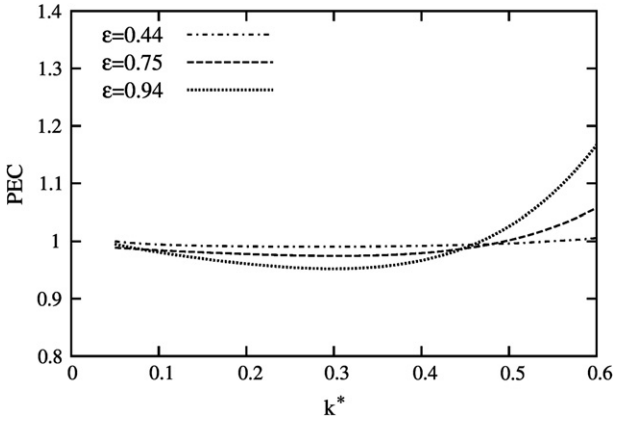

Fig. 10. Performance evaluation criteria. $F = 16$, $Re = 10$, $Pr = 7$, $\Lambda = 195$. Staggered arrangement.

$$\text{PEC} = H_r/H_{r\theta} \tag{64}$$

with

$$H_r = H - 2k_{eff} \quad H_{r\theta} = H - 2k_{eff\theta}$$

Fig. 10 reveals that PEC is slightly below 1 for $k^* < 0.46$ and for a value of the parameter F close to the experimental conditions. This means that the enhancement of the heat transfer coefficient does not compensate the increase in the friction factor in PEC for a microchannel with rough walls. However, PEC increases over 1 for slender rough elements, namely for $k^* > 0.46$, which corresponds to the case of a heat exchanger with pin fins. The numerical model shows that PEC also increases with the porosity in this situation, contrary to the case of $k^* < 0.46$.

6. Conclusions

Two different approaches were used in the present investigation for the purpose to predict the influence of roughness on heat transfer in fully-developed laminar flows through microchannels. The models considered parallelepipedic elements periodically distributed on the plane walls of a microchannel of infinite span. Three-dimensional numerical simulations were first conducted in a computational domain extending over one wavelength in streamwise and spanwise directions. A one-dimensional model (RLM model) was also developed on the basis of a discrete-element approach and the volume averaging technique. The closure problem of this semi-empirical model consisted in the determination of the drag and heat transfer coefficients of the rough elements as a function of the geometrical parameters of roughness. The three-dimensional numerical simulations revealed that this drag coefficient and, to a lesser extent, the heat transfer coefficient mainly depend on the porosity. As a result, these coefficients were obtained by means of a two-dimensional numerical modelling of the flow across banks of rods.

The numerical simulations and the RLM model agree to show that the Poiseuille number *Po* and the Nusselt number *Nu* increase with the relative roughness and are nearly independent of *Re* in the laminar regime ($Re < 2000$). Moreover, the increase in *Po* observed during previous experiments is well predicted both by the three-dimensional simulations and the RLM model [5], which tends to inspire confidence in the model.

The analysis revealed that the roughness effect may be interpreted by using effective roughness heights k_{eff} and $k_{eff\theta}$ or, equivalently, effective passage heights for this simplified situation. When normalized with the actual roughness height, these effective roughness heights depend on two dimensionless local parameters: ε, the porosity of the rough-layer and k/L, the roughness height normalized with the distance between the rough elements. The RLM model shows that k_{eff}/k and $k_{eff\theta}/k$ are independent of the relative roughness k^* at given k/L and may be simply approximated by laws of the form: $(k_{eff}/k) = 1 - (c(\varepsilon)/2\pi)(L/k)$ for $k/L > 0.2$. The constant c decreases with the porosity.

It is worth emphasizing that the roughness effects studied in the present work are especially expected in microdevices, where a significant level of relative roughness may result from fabrication

processes owing to the small size of the microsystems. The present model shows that roughness increases the friction factor more than the heat transfer coefficient and should be at most avoided during the fabrication of microchannels used for heat transfer. This conclusion is, however, reversed when microchannels are deliberately fabricated with fin pins for the purpose to improve heat transfer. In this last case, slender parallelepipedic fins ($k^* > 0.46$) are efficient to achieve a high transfer rate and give a performance evaluation criteria higher than 1.

This work could be easily extended to the influence of the solid/fluid conductivity ratio on the performance of a microchannel. Another important issue concerns the situation of developing flow and thermal fields where the axial conduction must be taken into account. This problem is more difficult than the current one since the velocity and temperature fields are no more periodic so that the simplified approaches used in this study do not apply. Three-dimensional numerical computations must then be extended to a large volume of the microchannel and the RLM model must be adapted to account for the unknown variations of the temperature associated with the slow variable.

A last issue concerns the possibility to apply the model to microdevices with inhomogeneous surface texture. More complex wall structures than a simple periodic distribution of identical elements may be investigated like in the numerical work of Croce and d'Agaro [17]. A first step was undertaken by considering a bimodal distribution of periodic structures consisting in two families of rough elements of significantly different sizes. The first results show that the friction coefficient is dominated by the structures of larger size, as expected, whereas the other family has a minor effect on the flow and the friction coefficient. This indicates that the maximum roughness height is the most important parameter to characterize the wall texture, at least for a first approximation, as also suggested by Fig. 8 when the rough-layer is rather compact. Further detailed studies are obviously needed to gain more precise insight on this issue.

Acknowledgements

Gabriel Gamrat was financially supported by the French Ministry of Education, which is gratefully acknowledged.

References

[1] G.L. Morini, Single-phase convective heat transfer in microchannels: a review of experimental results, Int. J. Thermal Sci. 43 (2004) 631–651.
[2] G.H. Mala, D. Li, Flow characteristics of water in microtubes, Int. J. Heat Fluid Flow 20 (1999) 142–148.
[3] D. Pfund, D. Rector, A. Shekarriz, A. Popescu, J. Welty, Pressure drop measurements in a microchannel, AIChE J. 46 (2000) 1496–1507.
[4] Z. Li, Y.L. He, G.H. Tang, W.Q. Tao, Experimental and numerical studies of liquid flow and heat transfer in microtubes, Int. J. Heat Mass Transfer 50 (2007) 3447–3460.
[5] G. Gamrat, M. Favre-Marinet, S. Le Person, R. Bavière, F. Ayela, An experimental study and modelling of roughness effects on laminar flow in microchannels, J. Fluid Mech. 594 (2008) 399–423.
[6] C.B. Sobhan, S.V. Garimella, A comparative analysis of studies on heat transfer and fluid flow in microchannels, Microscale Thermophys. Eng. 5 (2001) 293–311.
[7] G.P. Celata, M. Cumo, S.J. McPhail, G. Zummo, Single-phase laminar and turbulent heat transfer in smooth and rough microtubes, Microfluid Nanofluid. 3 (2007) 697–707.
[8] S. Grohmann, Measurement and modeling of single-phase and flow-boiling heat transfer in microtubes, Int. J. Heat Mass Transfer 48 (2005) 4073–4089.
[9] S.G. Kandlikar, S. Joshi, S. Tian, Effect of surface roughness on heat transfer and fluid flow characteristics at low Reynolds numbers in small diameter tubes, Heat Transfer Eng. 24 (3) (2003) 4–16.
[10] Z. Liu, C. Zhang, Y. Huo, X. Zhao, Flow and heat transfer in rough micro steel tubes, Exp. Heat Transfer 20 (2007) 289–306.
[11] W. Qu, G.M. Mala, D. Li, Heat transfer for water flow in trapezoidal silicon microchannels, Int. J. Heat Mass Transfer 43 (2000) 3925–3936.
[12] M.M. Rahman, Measurements of heat transfer in microchannel heat sinks, Int. Comm. Heat Mass Transfer 27 (4) (2000) 495–506.
[13] S. Shen, J.L. Xu, J.J. Zhou, Y. Chen, Flow and heat transfer in microchannels with rough wall surface, Energ. Convers. Manag. 47 (2006) 1311–1325.
[14] X.Y. Wu, Ping Cheng, An experimental study of convective heat transfer in silicon microchannels with different surface conditions, Int. J. Heat Mass Transfer 46 (2003) 2547–2556.
[15] J. Koo, C. Kleinstreuer, Liquid flow in microchannels: experimental observations and computational analyses of microfluidics effects, J. Micromech. Microeng. 13 (2003) 568–579.
[16] J. Koo, C. Kleinstreuer, Analysis of surface roughness effects on heat transfer in micro-conduits, Int. J. Heat Mass Transfer 48 (2005) 2625–2634.
[17] G. Croce, P. D'Agaro, Numerical analysis of roughness effect on microtube heat transfer, Superlattices Microstruct. 35 (2004) 601–616.
[18] G. Croce, P. D'Agaro, Numerical simulation of roughness effect on microchannel heat transfer and pressure drop in laminar flow, J. Phys. D Appl. Phys. 38 (2005) 1518–1530.
[19] G. Croce, P. D'Agaro, C. Nonino, Three-dimensional roughness effect on microchannel heat transfer and pressure drop, Int. J. Heat Mass Transfer 50 (2007) 5249–5259.
[20] J.S. Andrade Jr., E.A.A. Henrique, M.P. Almeida, M.H.A.S. Costa, Heat transport through rough channels, Physica A 339 (2004) 296–310.
[21] Y. Zeng, T.-S. Lee, P. Yu, H.-T. Low, Numerical study on the influence of surface roughness on fluid flow and mass transfer in a flat-plate microchannel bioreactor, Int. J. Modern Phys. C 18 (2) (2007) 131–155.
[22] G. Gamrat, Modélisation de l'hydrodynamique et des transferts de chaleur dans des microcanaux à parois rugueuses, Ph.D. thesis, INPG Grenoble University, 2007, http://tel.archives-ouvertes.fr/tel-00172333/fr/.
[23] G. Maranzana, I. Perry, D. Maillet, Mini-and micro-channels: influence of axial conduction in the walls, Int. J. Heat Mass Transfer 47 (2004) 3993–4004.
[24] Y. Hu, C. Werner, D. Li, Influence of three-dimensional roughness on pressure-driven flow through microchannels, J. Fluid Eng. 125 (2003) 871–879.
[25] R. Bavière, G. Gamrat, M. Favre-Marinet, S. Le Person, Modelling of laminar flows in rough-wall microchannels, J. Fluid Eng. 128 (2006) 734–741.
[26] R.P. Taylor, H.W. Coleman, B.K. Hodge, Prediction of turbulent rough-wall skin friction using a discrete-element approach, J. Fluid Eng. 107 (1985) 251–257.
[27] R.P. Taylor, H.W. Coleman, B.K. Hodge, Prediction of heat transfer in turbulent flow over rough surfaces, J. Heat Transfer 111 (1989) 568–572.
[28] S. Whitaker, Flow in porous media. I: a theoretical derivation of Darcy's law, Transport Porous Media 1 (1986) 3–25.
[29] Z. Guo, Z. Li, Size effect on microscale single-phase flow and heat transfer, Int. J. Heat Mass Transfer 46 (2003) 149–159.
[30] G. Gamrat, M. Favre-Marinet, S. Le Person, Numerical study of heat transfer over banks of rods in small Reynolds number cross flow, Int. J. Heat Mass Transfer 51 (2008) 853–864.
[31] B. Alazmi, K. Vafai, Analysis of fluid flow and heat transfer interfacial conditions between a porous medium and a fluid layer, Int. J. Heat Mass Transfer 44 (2001) 1735–1749.
[32] A.D. Stroock, S.K. Dertinger, G.M. Whitesides, A. Adjari, Patterning flows using grooved surfaces, Anal. Chem. 74 (2002) 5306–5312.
[33] R.L. Webb, Principles of Enhanced Heat Transfer, John Wiley & Sons, New York, 1994.